International Journal of Sediment Research 37 (2022) 97–109

Contents lists available at ScienceDirect

International Journal of Sediment Research

journal homepage: www.elsevier.com/locate/ijsrc

Original Research

Sediment dynamics in the mudbank of the Yangtze River Estuary under regime shift of source and sink

Dai Zhang [a], Weiming Xie [a], Jian Shen [b], Leicheng Guo [a], Yu Chen [a], Qing He [a, *]

[a] State Key Laboratory of Estuarine and Coastal Research, East China Normal University, Shanghai, 200241, China
[b] Virginia Institute of Marine Science, College of William & Mary, Gloucester Point, VA, 23062, USA

ARTICLE INFO

Article history:
Received 18 September 2020
Received in revised form
29 June 2021
Accepted 8 July 2021
Available online 31 July 2021

Keywords:
Sink-source shift
Fluvial sediment reduction
Sediment flux
Yangtze River Estuary

ABSTRACT

The southeastern portion of the Yangtze River Estuary (or Yangtze Estuary) was considered to be the deposition center and the mudbank of the Yangtze River Delta. As the fluvial sediment supply began to decline in the 1980s and the reduction accelerated after the completion of the Three Gorge Dam in 2003, more fluvial sediment was trapped decreasing the suspended sediment concentration (SSC) environment in the river mouth area. Moreover, the accretion rate of the mudbank has slowed down in recent decades. In fact, the mudbank shrank and has faced a regime shift from sediment sink to source. A better understanding of the tidal-scale dynamics and spatial variability of the system is essential to explore the conversion of the sediment sources and sinks in the Yangtze Estuary affected by natural variations and human activities. Flow velocity, salinity, and suspended-sediment concentration during spring and neap tides were measured at three sites on the mudbank in July 1982 and July 2013. The variation in flow was not significant at all the sites measured in the study area from 1982 to 2013. However, the sediment dynamics changed remarkably over these three decades. The temporal distribution of the SSC increased in the bottom layer. The SSC was much larger during the early flood tide period in 2013. The tidal range increased by nearly 10% and the flood dominance increased in the study area from 1982 to 2013. The salinity dynamics underwent a transition from a stratified system in 1982 to a well-mixed system in 2013. The landward sediment budget increased remarkably from 1982 to 2013. The decreased fluvial sediment supply, increased flood dominance, well-mixed salinity, and increased tidal range were directly responsible for the larger landward sediment budget and more severe erosion in the mudbank in 2013. The current results reveal the flow and sediment dynamics during the conversion of the sediment sink to source. Furthermore, it was determined that the sediment-starved process in the estuarine environment, which occurred due to the reduction in the fluvial sediment, leads to an increased landward transport of sediment. The current study provides a clear understanding of the mechanisms governing the delta system transition in the mudbank of the Yangtze Estuary, which is useful for delta protection in the future.

1. Introduction

Estuaries and deltas connect rivers with open oceans and represent an important component of the global sediment source and sink system. Riverine sediment is transported and deposited mostly in estuaries and deltas, which are either a final sedimentary sink or a passageway to the oceans (Guo et al., 2019; Stanley & Warne, 1994; Syvitski et al., 2009). Under natural conditions, the sediment source and sink system in estuaries and deltas can always reach an equilibrium state at an appropriate timescale. However, natural variations and human modifications have reached unprecedented levels during the last decades, thereby breaking the equilibria and modifying the evolution processes in estuaries and deltas. Many rivers worldwide have experienced a reduction in sediment flux primarily due to reservoir construction and other factors (Guo et al., 2018; Milliman & Farnsworth, 2011; Walling & Fang, 2003). For example, fluvial sediment entering the sea has now decreased to almost zero for the Nile Delta (Frihy et al., 2003); the Mississippi Delta has also lost about 70% of its fluvial sediment input (Milliman & Farnsworth, 2011). Human impacts, including the construction of navigational channels and reclamations, have greatly modified the physical environments of estuaries and play increasingly important roles in the delta evolution

* Corresponding author.
E-mail address: qinghe@sklec.ecnu.edu.cn (Q. He).

https://doi.org/10.1016/j.ijsrc.2021.07.005

(Cai et al., 2012; Luan et al., 2016; Ralston et al., 2019; Syvitski & Saito, 2007; Vellinga et al., 2014; Winterwerp et al., 2013). These changes introduce feedback that additionally alter hydrodynamic and sedimentary processes and lead to a regime shift to sediment source and sink systems in estuaries and deltas (Winterwerp et al., 2013).

The Yangtze River Estuary (or Yangtze Estuary) in China is ideal for examining estuarine regime shifts that occur in response to changes in both the upstream reach and deltaic regions. The Yangtze Estuary connects the longest river in China with the East China Sea, with an estuary width of almost 100 km. Chongming Island, Changxing Island, Hengsha Island, and the Jiuduansha Shoaldivide the estuary into four channels: the North Branch, North Channel, and North and South Passages (Fig. 1) (Xie et al., 2009). In the past century, estuaries have been developing seawards (Chen et al., 1985). For example, the 5 m isobath of the Nanhui Shoal has gradually expanded toward the sea at approximately 0.5–1.2 km/yr. During this progradation, the profile, slope, and curvature remained similar (Chen, 2007; Chen et al., 1985). A large flat area on the outskirts of the South Passage functions as the main conduit for the water and sediment of the Yangtze River (Milliman et al., 1985). This is because the tidal current force was relatively lower on the Nanhui Shoal. Therefore, sediment easily deposit when passing the area in the ebb or flood tides and part of the sediment that exited the Yangtze Estuary during ebb tide re-entered the Nanhui Shoal and entered the Yangtze Estuary during flood tide (Yun, 1983). Therefore, there is a mudbank outside the Nanhui Shoal, with a high sediment exchange ratio between the near-bottom suspended and sea-bottom sediments. The Nanhui Shoal is considered as one of the deposition centers and sediment sinks of the Yangtze River Delta (Liu et al., 2010; Stanley & Chen, 1993; Wei et al., 2017).

After the construction of more than 80,000 dams, the fluvial sediment supply has now decreased to less than 140 Mt/yr, which was 450 Mt/yr from 1969 to 1985 (Yang et al., 2018). Meanwhile, many deltaic engineering projects have been constructed in the Yangtze Estuary during recent decades for navigation, freshwater consumption, and wetland management purposes. There is serious siltation in the deep-water navigation channel along the North Passage, which requires extensive dredging every year.

Channels and shoals in the Yangtze Estuary were not isolated. Water and sediment exchanges frequently occurred between different channels and shoals, including the North Passage and the Nanhui Shoal. In the current study, the directions of the net sediment fluxes suggest that a large amount of sediment was transported to the South Passage (the turbidity maximum zone) from the study area. Previous studies have shown that the sediment deposited in the North Passage was delivered from the submerged delta. When sediment in the North Passage was dredged to the eastern Hengsha Shoal, more sediment would be delivered from the submerged delta to the North Passage to maintain the turbidity maximum zone. Due to the construction of training walls, the North Passage experienced net accretion of 17.2 Mm^3/yr in 1998–2011. The annual dredging volume was 47.2 Mm^3/yr in 2000–2012 and a considerable portion of the dredged sediment was used for siltation promotion of sedimentation and land reclamation at the adjacent shoals (Luan et al., 2016). The annual accretion volume at East Nanhui Mudflat reached 12 Mm^3/yr in 1998–2013 due to land reclamation. The fluvial sediment decreased while more sediment particles were delivered from the mudbank or the subaqueous delta to the shoals. Moreover, previous studies suggested that training walls enhanced the scouring capacity of tidal currents at the subaqueous delta, and, thereby, accelerated the erosion of the mudbank (Luan et al., 2018). Eroded sediment is transported to the North Passage by flood tide currents and erosion areas appeared around the delta front zone, including the mudbank (Zhu et al., 2016).

Previous studies have found that more sediment was delivered to the mudbank through channels during ebb tide periods as compared to the sediment transported away from the shoals during flood tide periods (Thomas et al., 2002; Yun, 1983). These processes resulted in sediment deposition in mudbanks. Moreover, increasing local engineering projects in the Yangtze Estuary were considered to play a dominant role compared to riverine

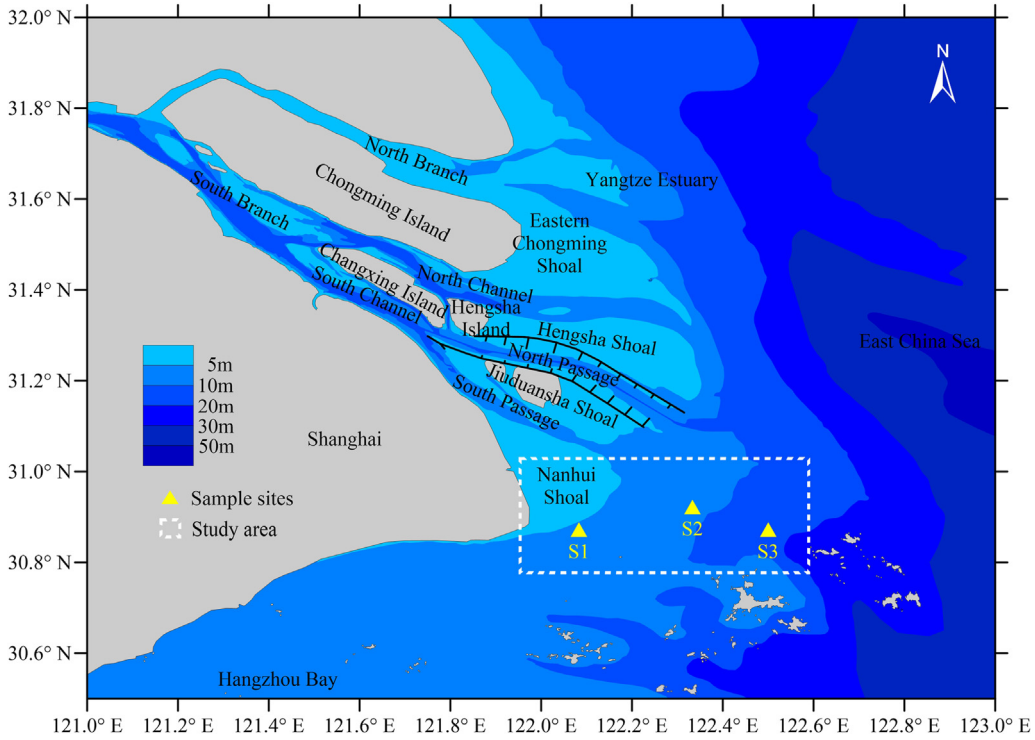

Fig. 1. Map of the Yangtze Estuary showing the locations of the sampling sites and the study area of bathymetric data analysis.

impacts on morphological changes of the river delta at a short-term timescale (year to decade) (Fan et al., 2017; Wei et al., 2017). However, the average suspended sediment concentration (SSC) has changed little in recent decades (Liu et al., 2014), which is not consistent with the severe morphological changes of the Yangtze Estuary (Luan et al., 2016; Zhu et al., 2019). A better understanding of the variation in sediment dynamics under new natural conditions and human impacts is still lacking and is indeed needed to explore the reason why the mudbank is converting from a sediment sink in the Yangtze River Estuary to a sediment source.

In the current study, two field datasets were collected in the mudbank of the Yangtze Estuary over a 31-year interval (in 1982 and 2013) to characterize its hydrodynamics and sediment dynamics (Fig. 1). Better understanding of the tidal-scale dynamics and spatial variability of the system are sought. The objectives of this study are to: (a) quantify the changes in hydrodynamics and calculate the residual sediment flux at different spatial and temporal scales; (b) discuss how the changing tidal asymmetry, salinity stratification, and sediment flux affect the deposition-erosion shift; and (c) determine the unsaturated sediment transport process in the mudbank, which was derived from the fluvial sediment reduction, and its role in the regime shift of the sink and source. The results of the current study can be used to understand sediment redistribution in estuaries when fluvial sediment loads decrease and assess the impact of the river reservoir and estuary projects on the water and sediment transport in the mudbank area, while providing guidance for other estuaries worldwide that exhibit similar conditions.

2. Study area

The Yangtze River is the longest river in Asia and the third-longest river in the world. The river forms four main distributaries within the delta. More than 95% of the water and sediment fluxes into the sea through the South Branch (Yang et al., 2018). The Yangtze Estuary receives an average of 893 km^3/yr of runoff and 368 Mt/yr of sediment load in the period 1950–2015 (Fig. 2). The variation in annual water runoff can be omitted in the past half-century, while the annual fluvial sediment supply declined continuously after the 1980s. The fluvial sediment supply has dropped to a notably low level in recent years (2003–2016, 135 Mt/yr), which is only 40% of that in 1982–2002 (Luan et al., 2018; Yang et al., 2018). The mean tidal range and wave height at the Yangtze River mouth are 2.67 m and 0.9 m, respectively (Yun, 2004). The seabed at the mouth bar area is dominated by cohesive sediment, which can be frequently resuspended by tidal currents (Liu et al., 2010).

Many engineering projects have been constructed in the estuary in recent decades. The largest one is the deep navigation channel project (DNCP), which comprises training wall construction and intensive channel dredging (Fig. 1). The DNCP was implemented from 1998 to 2010 and had important impacts on estuarine processes.

3. Methods

3.1. Data collection

Two vessel-based surveys of flow velocity, salinity, and SSC were done during the spring and neap tide periods in July 1982 and July 2013 (Table 1, Fig. 2). Each survey included three measuring sites (S1, S2, and S3) in the mudbank of the Yangtze Estuary, which is located outside the South Passage (Fig. 1) and has been reported as a fluvial sediment sink over the long term (Yun, 1983). The three sites in 1982 and 2013 almost overlapped. At each measuring site, the survey was operated continuously for approximately 27 h.

In 1982, the annual fluvial water and sediment fluxes into the sea were 957 km^3 and 467 Mt, respectively, which was close to the mean values for 1980–1984 (963 km^3 and 497 Mt). By contrast, the annual fluvial water and sediment fluxes into the sea were 787 km^3 and 117 Mt, respectively, in 2013 which was also close to the mean values for 2011–2015 (853 km^3 and 117 Mt). The results demonstrated the representativeness of the two measuring years of conditions in their respective time periods. Moreover, the study area was found to be the mudbank and the deposition center of the Yangtze Estuary by previous studies (Liu et al., 2010). The three measuring sites spatially covered the study area and could represent the mudbank of the Yangtze Estuary.

During the survey in 1982, all parameters at each station were measured in six layers (0.0h, 0.2h, 0.4h, 0.6h, 0.8h, and 1.0h, where h is the water depth). The velocity was recorded at intervals of 30 min. Salinity and SSC were measured using water samples with an interval of 30 min. During the survey in 2013, the salinity and SSC at each station were measured using an optical backscatter sensor (OBS, Campbell Scientific) for six layers (0.0h, 0.2h, 0.4h, 0.6h, 0.8h, and 1.0h) at intervals of 30 min. Velocity was recorded using an acoustic Doppler current profiler (ADCP, Teledyne Marine) with an interval of 30 min. The field measurements captured the decadal variability in the hydrodynamics and sediment dynamics in the mudbank.

Four sets of bathymetric maps were compiled (1978, 1986, 2010, and 2016) at uneven intervals to evaluate the morphological implications of the hydrodynamics and sediment dynamics. The maps were based on echo sounder measurements, with a vertical error of approximately 0.1 m (Zhao et al., 2018).

3.2. Data processing

During the survey in 1983, water samples were filtered, dried, and weighed to calculate the SSC. During the survey in 2013, the OBS data were calibrated by regressing against the measured SSC for each of the surveys. The quality of the OBS calibrations was suitable, with an average coefficient of determination (R^2) value of 0.94 at the three measuring sites. Digital elevation models (DEMs) with 100 m × 100 m grid resolutions derived from the bathymetric maps were produced using Kriging interpolation in the ArcGIS mapping software package (Xie et al., 2017).

3.3. Residual sediment flux calculation

The sediment fluxes were computed over the 27 h tidal cycles to interpret decadal variability. The study area is located in the open sea area; therefore, the velocity also was decomposed into east-west (E) or north-south (N) directions to better calculate sediment fluxes. Positive values along the east-west direction indicate eastward flow, while positive values along the north-south direction indicate flow toward the south.

The residual transport of water (Tr_w) and sediment (Tr_s) through a unit width along the east-west (E) or north-south (N) direction at the layer i ($i = 1, \ldots, 6$) can be defined as

$$\mathrm{Tr}_{wi}(\mathrm{E}) = \frac{1}{T}\int_0^T V(\mathrm{E})_i \cdot \Delta z \mathrm{d}t \tag{1}$$

$$\mathrm{Tr}_{wi}(\mathrm{N}) = \frac{1}{T}\int_0^T V(\mathrm{N})_i \cdot \Delta z \mathrm{d}t \tag{2}$$

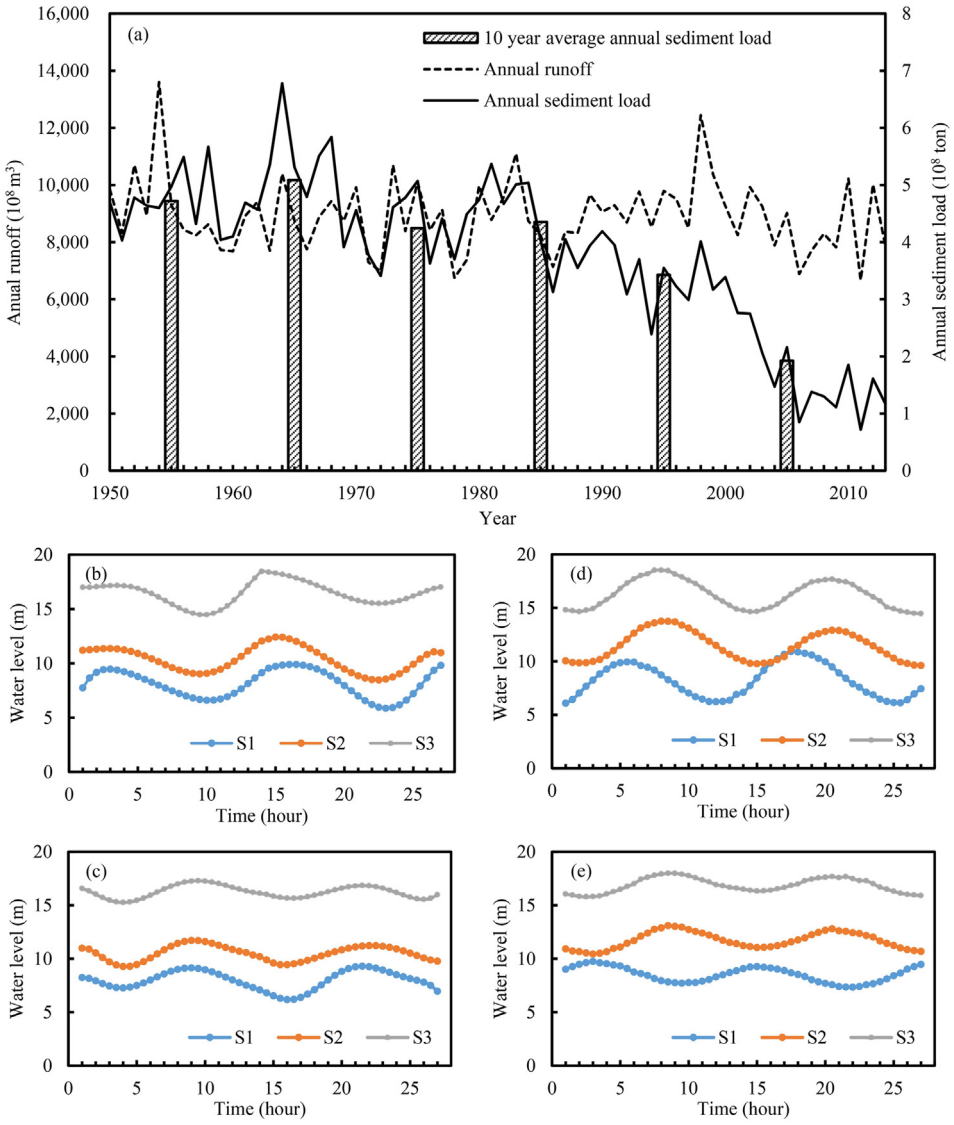

Fig. 2. (a) Annual runoff and sediment load in the Yangtze Estuary. The bars present the 10-year average annual sediment load. Measured water level during (b) spring tides in 1982, (c) neap tides in 1982, (d) spring tides in 2013, and (e) neap tides in 2013.

$$\mathrm{Tr}_{si}(\mathrm{E}) = \frac{1}{T}\int_0^T V(\mathrm{E})_i \cdot \mathrm{SSC}_i \cdot \Delta z \mathrm{d}t \tag{3}$$

$$\mathrm{Tr}_{si}(\mathrm{N}) = \frac{1}{T}\int_0^T V(\mathrm{N})_i \cdot \mathrm{SSC}_i \cdot \Delta z \mathrm{d}t \tag{4}$$

Table 1
Summary of the tidal surveys in the study area. The locations of the measuring sites are shown in Fig. 1.

Year	Site	Period	
		Spring tide survey	Neap tide survey
1982	S1	Jul 7 9:00 – Jul 8 11:00	Jun 30 10:00 – Jul 1 12:00
	S2	Jul 7 9:00 – Jul 8 11:00	Jun 30 9:00 – Jul 1 11:00
	S3	Jul 7 9:00 – Jul 8 11:00	Jun 30 10:00 – Jul 1 12:00
2013	S1	Jul 24 7:00 – Jul 25 9:00	Jul 30 14:00 – Jul 31 16:00
	S2	Jul 22 15:00 – Jul 23 17:00	Jul 29 7:00 – Jul 30 9:00
	S3	Jul 22 15:00 – Jul 23 17:00	Jul 29 7:00 – Jul 30 9:00

where $V(\mathrm{E})_i$ or $V(\mathrm{N})_i$is the current velocity along the east-west (E) or north-south (N) directions, respectively, at the ith layer, $\Delta z = H/6$ is the thickness of layer i, H is the total water depth that fluctuates with the tidal wave propagation, and SSC_i is the sediment concentration at the ith layer. If T represents the period of flood-ebb tidal cycles, then $\mathrm{Tr}_{w(s)i}(\mathrm{E})$ is the residual substance (water or sediment) transport of the ith layer (Wu et al., 2006).

3.4. The Richardson number calculation

To quantify the stratification of water, the Richardson number generally is used to characterize the stratification. The Richardson number (Ri), which is the ratio of buoyancy to shear production, signifies the degree of stratification and mixing in estuaries. Ri can be calculated as follows (Geyer & Smith, 1987):

$$Ri = \frac{-(g/\rho_\mathrm{w})(\partial\rho_\mathrm{w}/\partial z)}{(\partial u/\partial z)^2 + (\partial v/\partial z)^2} \tag{5}$$

where g is the gravitational acceleration, ρ_w is the density of estuarine water, z is the height above the bed, and u and v are the

eastern and northern velocity components, respectively. Both theory and observations indicate that in a stratified shear flow with $Ri < 0.25$ or $\log_{10}(Ri^{-1}) > 0.60$, the flow is unstable and the turbulent mixing is enhanced; however, when $Ri > 0.25$ or $\log_{10}(Ri^{-1}) < 0.60$, the flow is stable and the mixing is inhibited. In other words, the threshold can be used to separate two different turbulent regimes: strong and weak mixing. (Peters, 1997). The density of estuarine water can be calculated by considering salinity and SSC in the water column as follows (Winterwerp, 2001):

$$\rho_w = \rho_0 + \beta S \rho_0 + \left(1 - \frac{\rho_0 + \beta S \rho_0}{\rho_s}\right) c \quad (6)$$

where ρ_0 is the density of fresh water, ρ_s is the sediment density (2650 kg/m^3), β is a constant (7.8×10^{-4}), S is salinity (ppt), and c is the mass sediment concentration (kg/m^3).

4. Results

Table 2 lists an overview of the data derived from measurements at the three measuring sites in 1982 and 2013. SSC data during spring tide and salinity data during neap tide at S3 in1982 were unavailable. This was due to the damage of the water sample bottle. The mudbank is a flood-dominant tidal environment. However, tidal asymmetry decreased seaward in both years. The tidal asymmetry at the three measurement sites showed a declining trend in recent decades (Table 1). Both spring and neap tides were present in 1982 and 2013.

In the study area, the mean tidal range in 2013 was larger than that in 1982, particularly for S1 and S2. The maximum tidal range appeared at S1 in spring tides, which were 3.97 and 4.80 m in 1982 and 2013, respectively.

4.1. Currents

From 1982 to 2013, the variation in currents was negligible at all three measurement sites in the mudbank (Figs. 3 and 4). The current velocity during flood periods was higher than that during ebb periods. The maximum velocity exceeded 2 m/s, which always appeared during early flood and the late ebb stages. The tidal currents in the study area are displayed as rotary currents (Fig. 5), which were very different from the tidal currents in the channels. The current directions ranged from 260° to 360° during the flood tides. During ebb tides, the current direction changed from 50° to 150°.

The current velocity measurements showed an increasing trend landward (Table 2). The tidal average velocity in 1982 was 0.74 m/s, 0.60 m/s, and 0.55 m/s at S1, S2, and S3, respectively. In 2013, the average velocity was 0.72 m/s, 0.69 m/s, and 0.62 m/s at S1, S2, and S3, respectively.

4.2. Suspended sediment concentration

At the most landward site S1, SSC was highest compared to of the SSC at the other sites (Table 2). The SSC during the spring tide was much larger than that during the neap tide for all three measuring sites in 1982 and 2013 (Fig. 6). The average SSC was 1.33 and 0.50 g/L at sites S1 and S2, respectively, during the spring tide, while it was only 0.35 and 0.25 g/L at sites S1 and S2, respectively, during the neap tide in 1982. In 2013, the average SSC was 1.42, 0.60, and 0.27 g/L at sites S1, S2, and S3, respectively, during the spring tide, while it was only 0.37, 0.16, and 0.08 g/L at sites S1, S2, and S3, respectively, during the neap tide.

Table 2
Tidal range (m), tidal period (h), tidal average velocity (m/s), suspended sediment concentration (SSC; g/L), and salinity (ppt) at the measuring sites in the study area in 1982 and 2013. SSC data during spring tide and salinity data during neap tide at S3 in1982 were unavailable. This was because of the damage of the water sample bottle.

	Site	Period	1982		2013	
			Spring	Neap	Spring	Neap
Tidal range (m)	S1	–	3.97	3.12	4.80	2.41
	S2	–	3.38	2.42	3.98	2.66
	S3	–	3.97	2.03	3.88	2.20
Tidal period (h)	S1	Flood	4.50	5.25	4.75	6.00
		Ebb	7.50	6.75	7.25	6.00
	S2	Flood	5.00	5.75	5.75	5.50
		Ebb	7.00	6.25	6.25	6.50
	S3	Flood	4.50	5.25	6.00	5.75
		Ebb	7.50	6.75	6.00	6.25
Tidal average velocity (m/s)	S1	Flood	0.90	0.64	0.84	0.60
		Ebb	0.85	0.56	0.81	0.63
	S2	Flood	0.76	0.44	0.77	0.56
		Ebb	0.69	0.51	0.83	0.58
	S3	Flood	0.72	0.36	0.72	0.50
		Ebb	0.68	0.45	0.71	0.54
SSC (kg/m^3)	S1	Flood	1.33	0.28	1.45	0.36
		Ebb	1.33	0.41	1.38	0.39
	S2	Flood	0.51	0.25	0.67	0.18
		Ebb	0.50	0.24	0.54	0.14
	S3	Flood	–	0.13	0.29	0.09
		Ebb	–	0.12	0.24	0.08
Salinity (ppt)	S1	Flood	7.98	7.11	19.96	16.28
		Ebb	7.99	8.87	20.45	16.95
	S2	Flood	15.30	15.59	26.76	22.31
		Ebb	16.00	14.37	27.74	22.59
	S3	Flood	24.72	–	31.10	27.54
		Ebb	24.10	–	32.06	27.64

However, the difference in the temporal distributions of SSC was large between 1982 and 2013, particularly for spring tides (Figs. 6 and 7). At site S1, the temporal distribution of SSC was uniform with a higher SSC in the bottom layer during the entire spring tide in 1982 (Fig. 6); however, in 2013, the SSC was much larger during early flood periods. In 2013, the average SSC during the flood period was larger than that during the ebb period for all the measuring sites (Table 2).

4.3. Salinity

Salinity measurements showed an increasing trend seaward (Table 2). The average salinity in 1982 was 7.99, 15.32, and 24.41 ppt at S1, S2, and S3, respectively. In 2013, the average salinity was 18.41, 24.85, and 29.59 ppt at S1, S2, and S3, respectively. The difference in the average salinity was small between the flood period and ebb period for all measuring sites (Table 2). The salinity during the spring tide was larger than that during the neap tide.

From 1982 to 2013, the variation in salinity was large at all three sites in the study area (Figs. 7 and 8). The salinity in the study area markedly increased from 1982 to 2013 (Table 2). The vertical distribution of salinity was markedly stratified for all measuring sites in 1982, particularly for spring tides (Fig. 8a–e). However, the vertical distribution of salinity changed to well mixed in 2013 (Fig. 8g–l).

4.4. Sediment flux

On average, the volume of residual sediment flux at the three measuring sites in 1982 was much smaller than that in 2013 (Fig. 9). In 1982, the direction of residual sediment flux at site S1 was toward the river channel and the rate was 0.40 kg/(m·s) during the spring tide. The direction of residual sediment flux changed to seaward during the neap tide and the rate was 0.28 kg/(m·s)

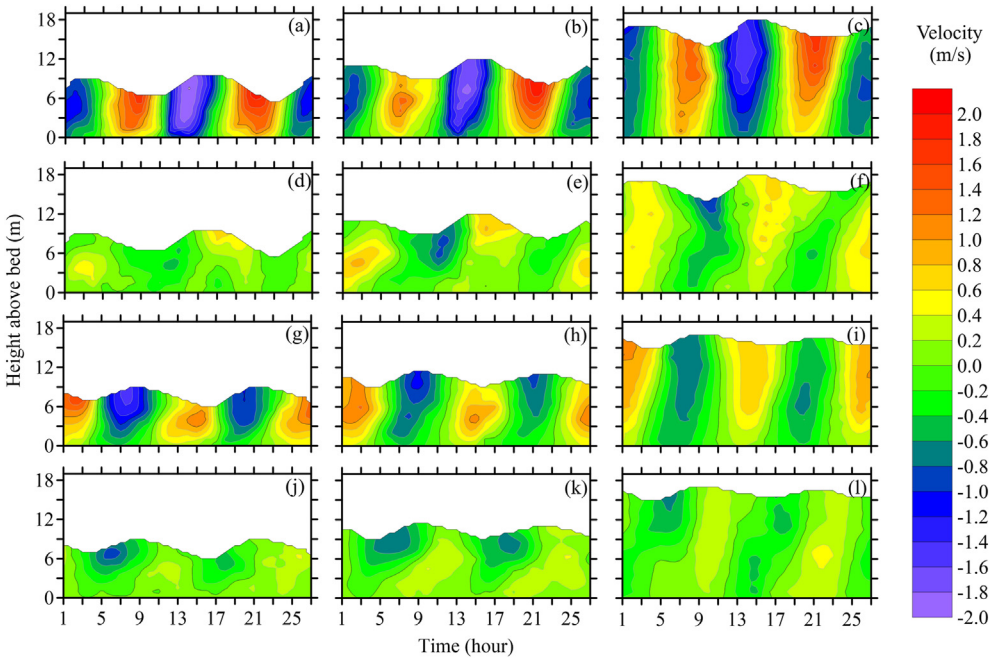

Fig. 3. Time series of velocity in 1982. Eastern component at (a) S1, (b) S2, and (c) S3 during the spring tide; Northern component at (d) S1, (e) S2, and (f) S3 during the spring tide; Eastern component at (g) S1, (h) S2, and (i) S3 during the neap tide; and Northern component in (j) S1, (k) S2, and (l) S3 during the neap tide.

(Table 3). The residual sediment flux at sites S2 and S3 were different from site S1, the directions of which were toward the south, even during spring tides (Fig. 9).

During the spring tide in 2013, the rate of residual sediment flux at site S1 increased greatly to 1.40 kg/(m·s) and the direction was still toward the river channel. This means that over the spring tides, there was a large net import of sediment from site S1 to the river mouth. The direction of the residual sediment flux at site S1 was also toward the river channel, even during the neap tides in 2013, at a rate of 0.05 kg/(m·s). At site S2, a large amount of sediment was transported southwest to Hangzhou Bay during both the spring and neap tides, the rates were 1.08 kg/(m·s) and 0.30 kg/(m·s), respectively (Fig. 9 and Table 3). The variation in the residual sediment flux at site S3 was small between 1982 and 2013.

Analysis of the surface and bottom residual sediment fluxes revealed that the surface residual sediment flux was significantly smaller than that of the bottom sediment. This is because the sediment in this area is mainly concentrated in the lower part of the water column. In 1982, the residual sediment flux at the bottom was very different and the residual sediment flux at the bottom was much larger than that at the surface, which corresponded to the distribution of the SSC at the bottom in 1982. In comparison, the

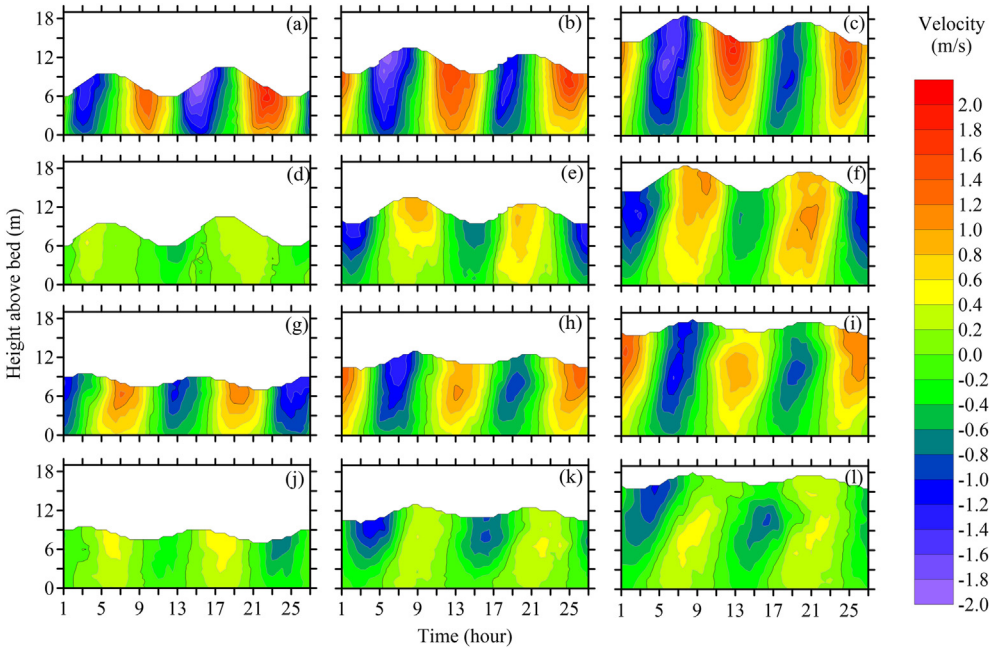

Fig. 4. Time series of velocity in 2013. Eastern component at (a) S1, (b) S2, and (c) S3 during the spring tide; Northern component at (d) S1, (e) S2, and (f) S3 during the spring tide; Eastern component at (g) S1, (h) S2, and (i) S3 during the neap tide; and Northern component in (j) S1, (k) S2, and (l) S3 during the neap tide.

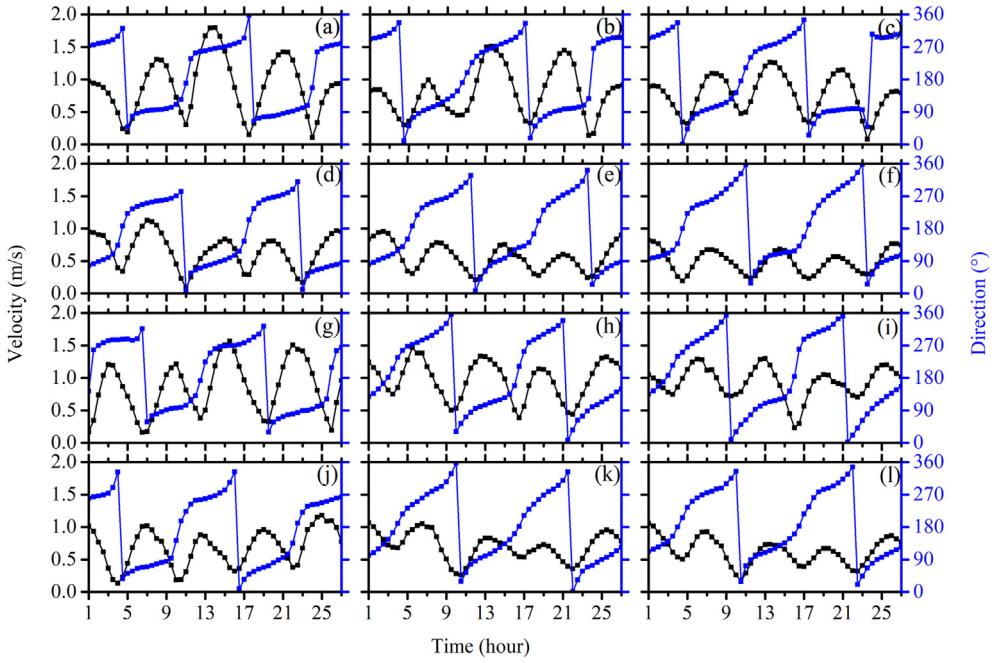

Fig. 5. Time series of average velocity and direction at (a) S1, (b) S2, and (c) S3 during the spring tide in 1982; (d) S1, (e) S2, and (f) S3 during the neap tide in 1982; (g) S1, (h) S2, and (i) S3 during the spring tide in 2013; and (j) S1, (k) S2, and (l) S3 during the neap tide in 2013.

difference in the amount of sediment transported between the surface and bottom layers in 2013 was much smaller, which is related to the fact that the bottom sediment is more likely to be suspended in the middle water layer.

4.5. Morphological change

Fig. 10 shows the topography of the study area in 1978, 1986, 2010, and 2016. In general, there was a landward increase in elevation from S3 to S1. The erosion and deposition patterns were obtained from the DEMs derived from the bathymetry by differencing the elevations from 1978, 1986, 2010, and 2016 (Fig. 11). The results indicated that the study area experienced critical changes during the recent decades from 1978 to 2016 (Table 4).

During 1978–1986, both erosion and deposition were observed in the study area (Fig. 11). Considerable deposition occurred in the area where the measurement sites were located. However, during 2010–2016, more severe erosion occurred throughout most of the study area, and the net erosion rate reached a very high rate of 7.2 cm/yr (Table 4).

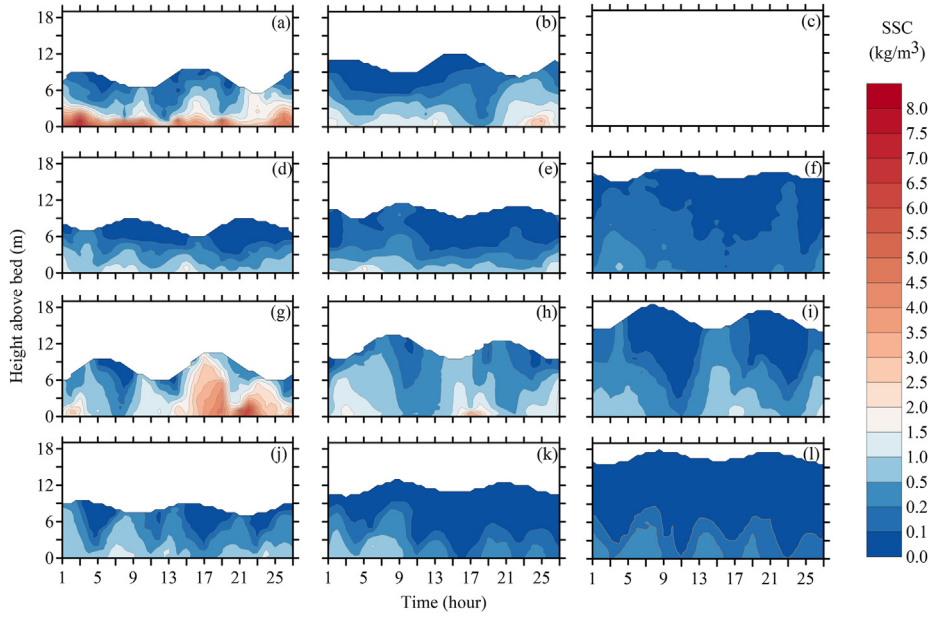

Fig. 6. Time series of SSC over water depth at (a) S1, (b) S2, and (c) S3 during the spring tide in 1982, the SSC data was unavailable at S3 due to the damage of water sample bottle; (d) S1, (e) S2, and (f) S3 during the neap tide in 1982; (g) S1, (h) S2, and (i) S3 during the spring tide in 2013; and (j) S1, (k) S2, and (l) S3 during the neap tide in 2013.

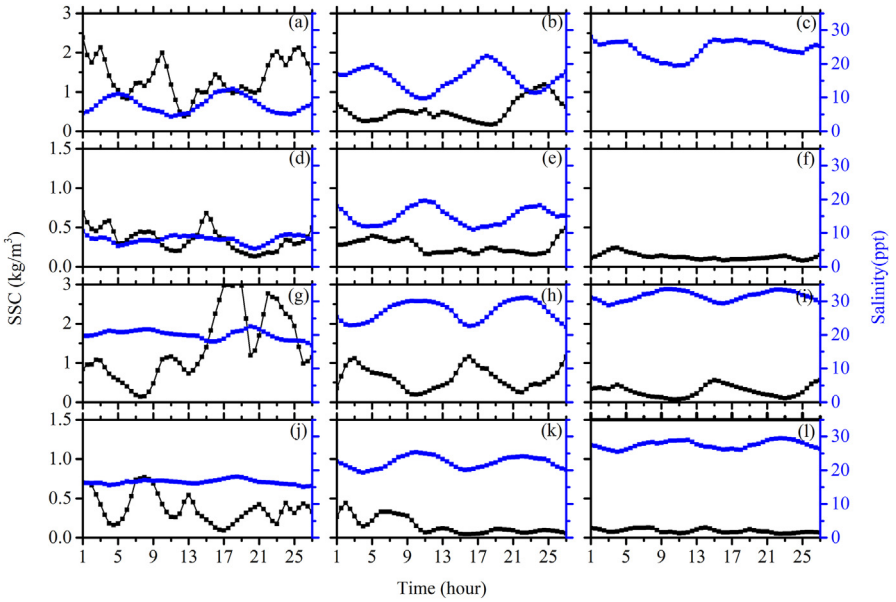

Fig. 7. Time series of average SSC and salinity at (a) S1, (b) S2, and (c) S3 during the spring tide in 1982, the SSC data was unavailable at S3 due to the damage of water sample bottle; (d) S1, (e) S2, and (f) S3 during the neap tide in 1982, the salinity data was unavailable at S3 due to the damage of water sample bottle; (g) S1, (h) S2, and (i) S3 during the spring tide in 2013; and (j) S1, (k) S2, and (l) S3 during the neap tide in 2013.

5. Discussion

5.1. Controls of sedimentary processes

5.1.1. Salinity stratification

Between 1982 and 2013, there were differences in the vertical distribution characteristics of SSC and salinity within the tide cycle, resulting in large differences in water layering. The stratification intensity indicated by *Ri* of water in the study area has changed over the past 30 years. The $\log_{10}(Ri^{-1})$ at S1 in 1982 mostly was less than 0.6, indicating that strong stratification and weak mixing occurred at S1 in 1982, which was also consistent with the distribution of the SSC. The high SSC was mainly concentrated in the bottom layer. The $\log_{10}(Ri^{-1})$ during the high tide at S1 in 2013 changed with water levels, and was less than 0.6 near the slack water, indicating the strongest stratification. The stratification at S2 was weaker than at S1 both in 1982 and 2013. In summary, $\log_{10}(Ri^{-1})$ (red dotted line in Fig. 12) in 1982 was generally smaller than that in 2013, indicating that the stratification intensity of the water body in 2013 was weaker compared to 1982.

During tidal periods in 1982, the SSC in the mudbank was not correlated with velocity on both flood and ebb tides (Fig. 6a–f),

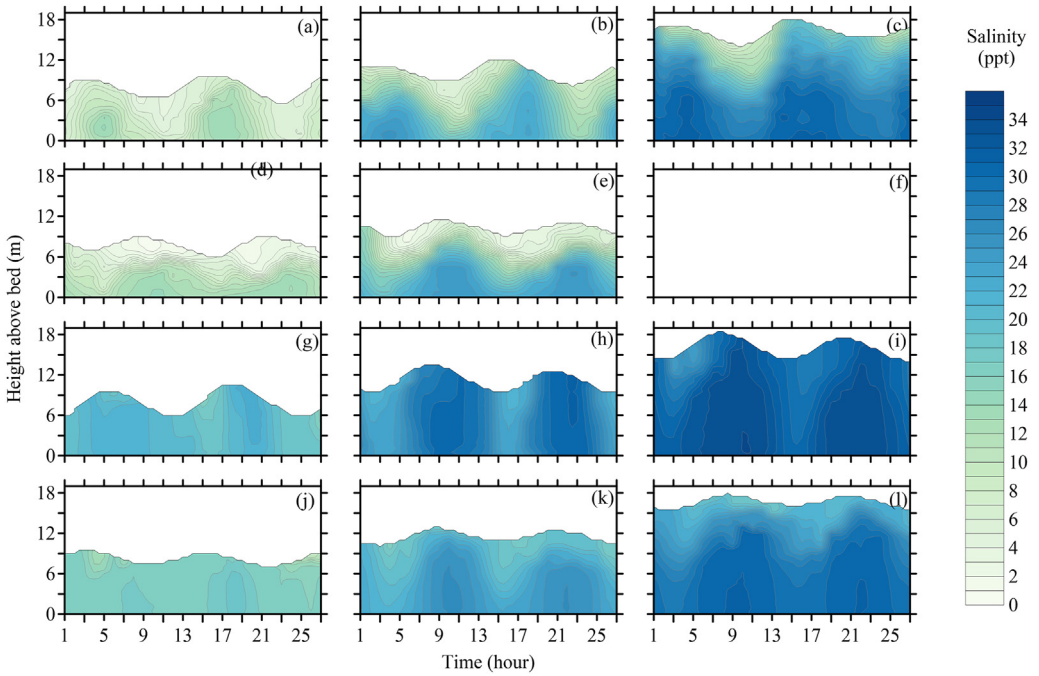

Fig. 8. Time series of salinity over water depth at (a) S1, (b) S2, and (c) S3 during the spring tide in 1982; (d) S1, (e) S2, and (f) S3 during the neap tide in 1982, the salinity data was unavailable at S3 due to the damage of water sample bottle; (g) S1, (h) S2, and (i) S3 during the spring tide in 2013; and (j) S1, (k) S2, and (l) S3 during the neap tide in 2013.

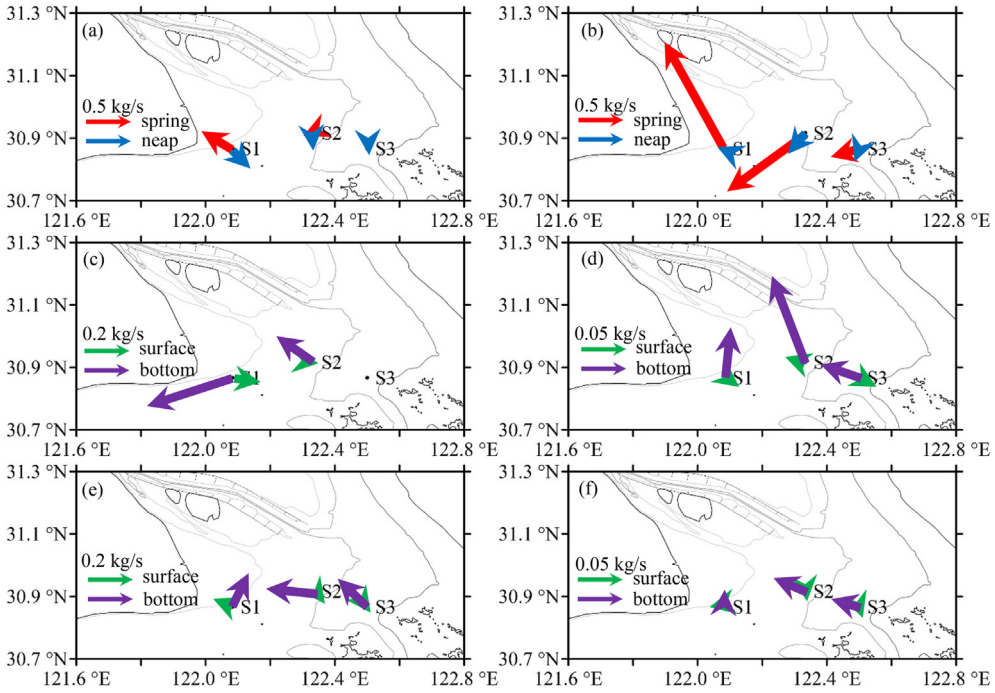

Fig. 9. Residual sediment flux in the study area during the spring tide and the neap tide: (a) vertical average residual sediment flux in 1982 and (b) vertical average residual sediment flux in 2013, (c) residual sediment flux of the surface and bottom layers during spring tide in 1982, (d) residual sediment flux of the surface and bottom layers during neap tide in 1982, (e) residual sediment flux of the surface and bottom layers during spring tide in 2013, and (f) residual sediment flux of the surface and bottom layers during neap tide in 2013. Flux result during spring tide at S3 in1982 was unavailable. This was because of the damage of the water sample bottle and SSC data during spring tide was missing.

with higher values being observed in the bottom layer owing to the strong salinity stratification. The salinity stratification shielded the seabed from high bed stresses, and the SSC in the upper layer was substantially lower than that in the bottom layer (Scully et al., 2011). This SSC distribution meant that sediment from local resuspension was rarely transported to other places but deposited in the study area. Meanwhile, the fluvial sediment easily settled in the study area because of the well-stratified environment (Geyer et al., 2001). In contrast, during tidal periods in 2013, the SSC in the mudbank was closely related to velocity (Fig. 6g–l), with higher SSC values appearing in early flood and late ebb tide periods owing to the higher velocities. The salinity was well mixed vertically over the water depth, indicating that high turbulence and strong bed shear stress occurred, leading to remarkable local sediment resuspension (Wu & Wu, 2018). Moreover, the value of the SSC was low at the beginning of the tidal period in 2013, indicating that little sediment was delivered from the area adjacent to the study area (Fig. 6). This sediment sourcing meant that the seabed in the study area was eroded and that the sediment was transported and deposited to other places such as Hangzhou Bay or tidal flats in the river mouth area. Weak salinity stratification resulted in more sediment resuspension in 2013 than in 1982.

5.1.2. *Tidal asymmetry and tidal range*

Tidal asymmetry, depending on the difference between flood and ebb tides, is important for sedimentary processes in estuaries

Table 3
Sediment flux per unit length [kg/(m·s)] and direction (Dir., °) at the measuring sites in the study area in 1982 and 2013. Flux results during spring tide at S3 in1982 were unavailable. This was because of the damage of the water sample bottle and SSC data during spring tide were missing.

Site	Period		1982		2013	
			Spring	Neap	Spring	Neap
S1	Flood	Flux [kg/(m·s)]	9.70	1.66	11.83	2.18
		Dir. (°)	274.92	252.85	278.18	257.16
	Ebb	Flux [kg/(m·s)]	7.91	1.91	9.98	2.19
		Dir. (°)	92.50	87.72	85.42	75.47
	Per tidal cycle	Flux [kg/(m·s)]	0.40	0.28	1.40	0.05
		Dir. (°)	301.09	135.07	331.87	294.44
S2	Flood	Flux [kg/(m·s)]	4.02	1.32	6.29	1.43
		Dir. (°)	278.11	261.11	277.89	266.42
	Ebb	Flux [kg/(m·s)]	3.38	1.29	4.73	1.06
		Dir. (°)	100.01	99.41	115.93	110.00
	Per tidal cycle	Flux [kg/(m·s)]	0.11	0.21	1.08	0.30
		Dir. (°)	245.88	176.43	234.21	220.43
S3	Flood	Flux [kg/(m·s)]	–	0.77	3.31	0.88
		Dir. (°)	–	275.24	287.14	274.77
	Ebb	Flux [kg/(m·s)]	–	0.89	2.68	0.81
		Dir. (°)	–	101.77	114.36	116.68
	Per tidal cycle	Flux [kg/(m·s)]	–	0.05	0.32	0.16
		Dir. (°)	–	176.58	254.54	201.08

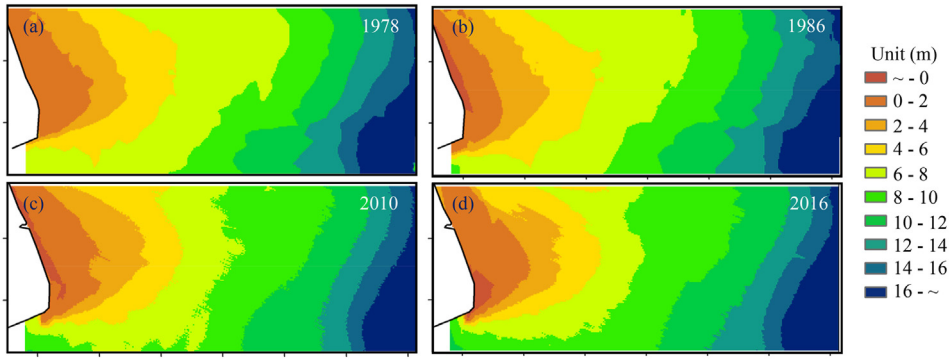

Fig. 10. Bathymetric maps at the study area in 1978, 1986, 2010, and 2016.

(Dronkers, 1986; Scully & Friedrichs, 2007; Wang et al., 2002). The flood dominancy was colculated using the following formula below (Chen et al., 1988).

$$R_Q = \left[Q_f \Big/ \left(Q_e + Q_f\right)\right] \times 100\% \tag{7}$$

where Q_f is the flood tide discharge and Q_e is the ebb tide discharge, $R_Q > 50\%$ indicates flood dominancy while $R_Q < 50\%$ represents ebb dominancy.

The results are listed in Table 5. Previous studies have also demonstrated that the study area was in a flood-dominated environment (Guo et al., 2015). The duration of the ebb tide period was markedly longer than that of the flood tide period, particularly for 1982. However, tidal asymmetry reduced from 1982 to 2013 (Table 2). The duration of the ebb tide period was equal to that of the flood tide period at site S3 in 2013. This had an important impact on sedimentary processes.

The difference in the average velocity and SSC was small in the study area from 1982 to 2013 (Table 2). In contrast, the residual sediment flux in the study area varied markedly between the two years. The residual sediment flux was small at all three sites in 1982 (Fig. 9). Clear evidence has shown that small variability in the SSC occurred during the tidal period (Fig. 7). The flood tide period was much shorter than the ebb tide period in a flood-dominated environment. As a result, less sediment was delivered to the river channel. In 2013, tidal asymmetry was reduced and flood dominance was stronger. The longer flood duration combined with high SSC values led to severe net sediment transport at S1 and S2 (Fig. 9). The tidal asymmetry and increased flood-dominance led to more sediment transport to the river mouth or Hangzhou Bay in 2013 compared to those in 1982.

Moreover, the tidal range increased in the study area from 1982 to 2013. The vegetation growth in the coastal wetlands always expands with an increasing tidal range, resulting in more sediment being deposited in the shoals. Previous studies have reported that coastal tidal flats experience accretion with increasing tidal range, which implies that more sediment would be transported from the adjacent sea to the coast (Kirwan & Guntenspergen, 2010). This process could lead to erosion occurring in the adjacent seabed.

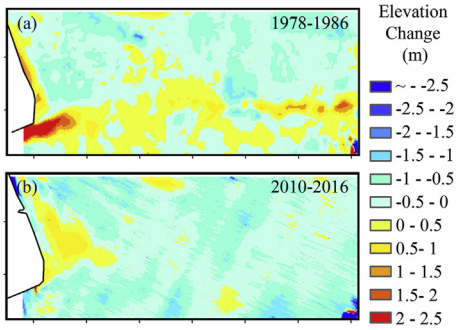

Fig. 11. Morphological changes in the study area during (a) 1978–1986 and (b) 2010–2016. The location of the study area is shown in Fig. 1.

5.1.3. Sediment carrying capacity

The sediment-carrying capacity was used to calculate the amount of sediment transported for the given flow and boundary conditions (Tan et al., 2018). Dou et al. (1995) introduced a sediment-carrying capacity formula using a large amount of experimental data obtained by the Nanjing Hydraulic Research Institute (NHRI) and field data from the Yangtze Estuary

$$S_* = \alpha \frac{\gamma\gamma_s}{\gamma_s - \gamma} \frac{n^2 U^3}{h^{4/3}\omega} \tag{8}$$

where $\alpha = 0.023$, S_* is the sediment-carrying capacity, γ_s and γ are the specific weights for sediment and water, respectively, n is Manning's roughness coefficient, which is 0.005 in the study area, U is depth-averaged velocity, and h is the water depth. Additionally, ω is the sediment settling velocity, which can be calculated from the modified formulation based on Stokes' law (Stokes, 1851):

$$\omega = \frac{1}{18} \frac{\gamma_s - \gamma}{\gamma} \frac{gD^2}{\nu} \tag{9}$$

where g is the gravitational acceleration ($g = 9.8$ m/s^2), D is the median grain size of the suspended sediment, and ν is the kinematic viscosity of water ($\nu = 1.10 \times 10^{-6}$ m^2/s). Field measurements showed that the median grain size of the suspended sediment was 5 μm in the study area in 2013. The median grain size was 6 μm in 1982, based on previous studies (Chen et al., 1988).

The calculated sediment-carrying capacity, S_*, increased by 13%–262% at the three measurement sites from 1982 to 2013

Table 4
Statistics of the erosion and deposition area and volume and net change rate in the study area. Positive values represent deposition, and negative values represent erosion.

		1978–1986	2010–2016
Erosion	Area (%)	70.1	89.7
	Volume (10^6 m^3/yr)	−57.1	−129.1
Deposition	Area (%)	29.9	16.0
	Volume (10^6 m^3/yr)	23.2	9.6
Net	Volume (10^6 m^3/yr)	−33.9	−119.5
	Rate (cm/yr)	−2.0	−7.2

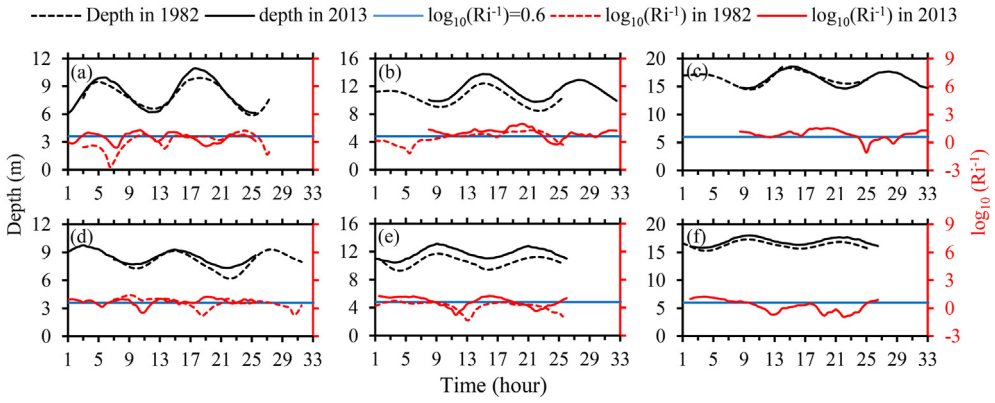

Fig. 12. Time series of Richardson number (*Ri)* at (a) S1, (b) S2, and (c) S3 during the spring tide; (d) S1, (e) S2, and (f) S3 during the neap tide, the Richardson number was unavailable at S3 in 1982, this was because of the damage of the water sample bottle, the SSC data during the spring tide and salinity data during the neap tide in 1982 were missing, and the density of estuarine water can't be calculated.

Table 5
The flood dominancy of the study area in 1982 and 2013.

Year	S1 Spring	S1 Neap	S2 Spring	S2 Neap	S3 Spring	S3 Neap
1982	53.2%	55.5%	54.1%	48.0%	50.7%	48.4%
2013	54.1%	50.8%	51.0%	49.3%	55.0%	48.0%

(Table 6). A higher S_* value led to a larger amount of sediment transport, which indicates that more sediment was eroded and transported in 2013 compared to the conditions in 1982. It should be noted that the SSC increased by 3%–31% during spring tides from 1982 to 2013, while it decreased by 5%–42% during neap tides. In 1982, the direction of residual sediment flux at site S1 was toward the river channel and the rate was 0.40 kg/(m·s) during the spring tide. The direction of residual sediment flux changed to seaward during the neap tide and the rate was 0.28 kg/(m·s). During the spring tide in 2013, the rate of residual sediment flux at site S1 increased greatly to 1.40 kg/(m·s) and the direction was still toward the river channel. The direction of the residual sediment flux at site S1 was also toward the river channel, even during the neap tides in 2013, at a rate of 0.05 kg/(m·s). More sediment was transported from the mudbank to the river channel. Moreover, the larger sediment-carrying capacity was accompanied by reduced SSC, resulting in unbalanced sediment transport and erosion in the study area in 2013. The reduction in fluvial sediment supply accelerated the 'sediment-starved' process in the mudbank of the Yangtze Estuary. More eroded sediment was transported from the mudbank to the Nanhui Shoal and the river mouth area because of the larger sediment-carrying capacity.

5.2. Conversion of the sink to source in the mudbank

Nearly 50 m of modern sediment was deposited in the mudbank of the Yangtze Estuary, which was considered as the deposition center and the sediment sink of the Yangtze River Delta (Liu et al., 2010; Stanley & Chen, 1993). As the fluvial sediment supply began to decline in the 1980s because more fluvial sediment was trapped in upstream reservoirs, in order to maintain a high SSC environment in the river mouth area, the accretion rate in the mudbank slowed down in the 1990s (Luan et al., 2016). Generally, delta deposition or erosion depends on the sediment budget between the fluvial sediment supply and offshore dispersal (Syvitski & Saito, 2007). Under decreasing fluvial sediment supply and relatively stable dispersal by coastal currents (Deng et al., 2017), the conversion from deposition to erosion in the Yangtze River Delta seems inevitable (Luan et al., 2018). This meant that the previous mudbank sediment sink would change to be the sediment source for the mouth bar area.

The Yangtze River Delta has been heavily influenced by large-scale estuarine engineering projects in recent decades, such as the Deep Navigation Channel Project (DNCP) and Eastern Hengsha Shoal Reclamation (EHSR). Previous studies have suggested that the training walls of the DNCP enhanced the scouring capacity of tidal currents at the subaqueous delta, thereby accelerating erosion of the mudbank (Luan et al., 2018). The annual dredging volume of the DNCP was 47.2 Mm^3/yr in 2000–2012 (Luan et al., 2016) and most of the sediment was used for land reclamation in the project EHSR. These processes subsequently accelerated the conversion of the sink to source in the mudbank.

This conversion process of the sink to source led to correlated changes in sedimentary processes in the study area. An integrated conceptual model describing the sedimentary processes in the study area (Fig. 13) has been developed here. In this way, sedimentary processes in the study area can be inferred as follows:

1) In 1982, the rich fluvial sediment was transported to the mudbank during the ebb tide period and deposited therein. The duration of flood was short and the sediment could not be delivered far away; consequently, it was deposited in the

Table 6
Statistics of the sediment carrying capacity at the measurement sites in the study area in 1982 and 2013.

	Site	Period	1982		2013	
			Spring	Neap	Spring	Neap
Sediment carrying capacity (kg/m^3)	S1	Flood	11.38	4.30	12.89	4.91
		Ebb	12.12	3.33	14.48	6.12
	S2	Flood	5.01	0.98	6.66	2.56
		Ebb	4.51	1.72	9.50	3.07
	S3	Flood	2.41	0.31	3.48	1.13
		Ebb	2.23	0.64	3.67	1.52

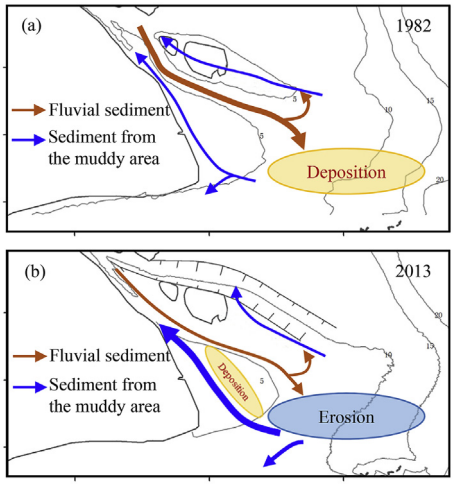

Fig. 13. Conceptual model for the sedimentary process in the mudbank of the Yangtze Estuary (a) in 1982 and (b) in 2013.

adjacent shoals. This resulted in the sedimentation on the mudbank and the coastal tidal flats.

2) In 2013, reduced fluvial sediment wasdelivered to the mudbank during the ebb tide period. However, the increasing scouring capacity of tidal currents and the well-mixed salinity environment made it difficult for sediment to settle down. Instead, the seabed was eroded. Due to the reduced ebb-dominance, more sediment was transported landward during the longer flood period and deposited in the coastal tidal flats, the deep navigation channel, and Hangzhou Bay.

6. Conclusions

The current study presented water column and sediment time-series of field observations for the mudbank of the Yangtze River Estuary. Two vessel-based surveys were done in July 1982 and July 2013 to reveal the hydrodynamics and sediment dynamics during recent decades, and the measurements included flow velocity, water level, salinity, and SSC. Bathymetric data were analyzed to evaluate morphological implications. The results expand the present understanding of the conversion of the sediment sink to a source in large deltas under natural variations and human impacts. The current findings are as follows:

1) In the study area, the mean tidal range in 2013 was larger than that in 1982, particularly for site S1. The maximum tidal range appeared at S1 in spring tides, which were 3.97 and 4.80 m in 1982 and 2013, respectively. The larger tidal range played an important role in increasing sediment trapping and accretion of coastal tidal flats. The ebb tide dominance in the study area decreased from 1982 to 2013.
2) The variation in flow was negligible at all the sites in the study area from 1982 to 2013. However, the sediment dynamics markedly changed over the three decades. The temporal distribution of SSC was even higher in the bottom layer, while in 2013, the SSC was much larger during early flood tide periods. The salinity dynamics underwent a comprehensive regime change between 1982 and 2013. This change was highlighted by the transition from a significantly stratified system in 1982 to a well-mixed system in 2013.
3) The volume of sediment flux at the three sites in 2013 was much larger than that in 1982. The residual sediment flux at site S1 in 2013 was three times higher than that in 1982. This resulted in more severe erosion in the study area. The bathymetric analysis showed that the net erosion rate was −2.0 cm/yr in 1978–1986 while it was −7.2 cm/yr in 2010–2016.
4) The changing tidal asymmetry, salinity stratification, and tidal range, which were deeply influenced by both natural variations and human impacts, controlled the sedimentary processes and convension of the sediment sink to source in the study area. The reduction in fluvial sediment supply and local estuarine engineering projects reshaped the delta environment and led to a reduced ebb tide dominance, well-mixed salinity, and an increased tidal range. The mudbank, which was the former sediment sink, eroded to maintain a high SSC in the mouth bar area and transitioned to the sediment source in recent years.

Declaration of competing interest

The authors declare that they have no known competing financial interests or personal relationships that could have appeared to influence the work reported in this paper.

Acknowledgments

The current study is supported by the National Natural Science Foundation of China (Grant Nos. 51739005, U2040216), and the Science and Technology Commission of Shanghai Municipality (Grant Nos. 20DZ1204700, 19QA1402900), and the project “Coping with deltas in transition” within the Programme of Strategic Scientific Alliance between China and the Netherlands (PSA), financed by the Ministry of Science and Technology (MOST), P.R. China (Grant No. 2016YFE0133700) and the Royal Netherlands Academy of Arts and Sciences (KNAW) (Grant No. PSA-SA-E-02).

References

Cai, H., Savenije, H. H. G., Yang, Q., Ou, S., & Lei, Y. (2012). Influence of river discharge and dredging on tidal wave propagation: Modaomen Estuary case. *Journal of Hydraulic Engineering, 138*(10), 885–896.

Chen, J. (2007). *Research and practice of estuary and coast in China*. Beijing, China: Higher Education Press. *(In Chinese)*

Chen, J., Shen, H., & Yun, C. (1988). *The morphodynamic process of the Yangtze Estuary*. Shanghai, China: Shanghai Scientific and Technical Publishers. *(In Chinese)*

Chen, J., Zhu, H., Dong, Y., & Sun, J. (1985). Development of the changjiang estuary and its submerged delta. *Continental Shelf Research, 4*(1/2), 47–56.

Deng, B., Wu, H., Yang, S., & Zhang, J. (2017). Longshore suspended sediment transport and its implications for submarine erosion off the Yangtze River Estuary. *Estuarine, Coastal and Shelf Science, 190*, 1–10.

Dou, G., Dong, F., & Dou, X. (1995). The sediment carrying capacity of tidal currents and waves. *Chinese Science Bulletin, 40*(5), 443–446. *(In Chinese)*

Dronkers, J. (1986). Tidal asymmetry and estuarine morphology. *Netherlands Journal of Sea Research, 20*(2), 117–131.

Fan, D., Wu, Y., Zhang, Y., Burr, G., Huo, M., & Li, J. (2017). South flank of the Yangtze delta: Past, present, and future. *Marine Geology, 392*, 78–93.

Frihy, O. E., Debes, E. A., & El Sayed, W. R. (2003). Processes reshaping the Nile delta promontories of Egypt: Pre- and post-protection. *Geomorphology, 53*(3–4), 263–279.

Geyer, W. R., & Smith, J. D. (1987). Shear instability in a highly stratified estuary. *Journal of Physical Oceanography, 17*(10), 1668–1679.

Geyer, W. R., Woodruff, J. D., & Traykovski, P. (2001). Sediment transport and trapping in the hudson River Estuary. *Estuaries, 24*(5), 670.

Guo, L., Su, N., Townend, I., Wang, Z. B., Zhu, C., Wang, X., Zhang, Y., & He, Q. (2019). From the headwater to the delta: A synthesis of the basin-scale sediment load regime in the changjiang river. *Earth-Science Reviews, 197*, 102900.

Guo, L., Su, N., Zhu, C., & He, Q. (2018). How have the river discharges and sediment loads changed in the Changjiang River basin downstream of the Three Gorges Dam? *Journal of Hydrology, 560*, 259–274.

Guo, L., van der Wegen, M., Jay, D. A., Matte, P., Wang, Z. B., Roelvink, D., & He, Q. (2015). River-tide dynamics: Exploration of nonstationary and nonlinear tidal behavior in the Yangtze River estuary. *Journal of Geophysical Research: Oceans, 120*(5), 3499–3521.

Kirwan, M. L., & Guntenspergen, G. R. (2010). Influence of tidal range on the stability of coastal marshland. *Journal of Geophysical Research: Earth Surface, 115*(F2), 2156–2202.
Liu, H., He, Q., Wang, Z., Weltje, G. J., & Zhang, J. (2010). Dynamics and spatial variability of near-bottom sediment exchange in the Yangtze Estuary, China. *Estuarine, Coastal and Shelf Science, 86*(3), 322–330.
Liu, J. H., Yang, S. L., Zhu, Q., & Zhang, J. (2014). Controls on suspended sediment concentration profiles in the shallow and turbid Yangtze Estuary. *Continental Shelf Research, 90*, 96–108.
Luan, H. L., Ding, P. X., Wang, Z. B., Ge, J. Z., & Yang, S. L. (2016). Decadal morphological evolution of the Yangtze Estuary in response to river input changes and estuarine engineering projects. *Geomorphology, 265*, 12–23.
Luan, H. L., Ding, P. X., Wang, Z. B., Yang, S. L., & Lu, J. Y. (2018). Morphodynamic impacts of large-scale engineering projects in the Yangtze River delta. *Coastal Engineering, 141*, 1–11.
Milliman, J. D., & Farnsworth, K. L. (2011). *River discharge to the coastal ocean – a global synthesis*. Cambridge, U.K.: Cambridge University Press.
Milliman, J. D., Shen, H., Yang, Z., & Meade, R. H. (1985). Transport and deposition of river sediment in the Changjiang Estuary and adjacent continental shelf. *Continental Shelf Research, 4*(1/2), 37–45.
Peters, H. (1997). Observations of stratified turbulent mixing in an estuary: Neap-to-spring variations during high river flow. *Estuarine, Coastal and Shelf Science, 45*(1), 69–88.
Ralston, D. K., Talke, S., Geyer, W. R., Al Zubaidi, H. A. M., & Sommerfield, C. K. (2019). Bigger tides, less flooding: Effects of dredging on barotropic dynamics in a highly modified estuary. *Journal of Geophysical Research: Oceans, 124*(1), 196–211.
Scully, M. E., & Friedrichs, C. T. (2007). The importance of tidal and lateral asymmetries in stratification to residual circulation in partially mixed estuaries. *Journal of Physical Oceanography, 37*(6), 1496–1511.
Scully, M. E., Geyer, W. R., & Trowbridge, J. H. (2011). The influence of stratification and nonlocal turbulent production on estuarine turbulence: An assessment of turbulence closure with field observations. *Journal of Physical Oceanography, 41*(1), 166–185.
Stanley, D. J., & Chen, Z. (1993). Yangtze delta, eastern China: 1. Geometry and subsidence of holocene depocenter. *Marine Geology, 112*(1), 1–11.
Stanley, D. J., & Warne, A. G. (1994). Worldwide Initiation of Holocene marine deltas by deceleration of sea-level rise. *Science, 265*(5169), 228–231.
Stokes, G. G. (1851). On the effect of the internal friction of fluids on the motion of pendulums. *Trans. Cambridge Philos. Soc., 9*(2), 8–106.
Syvitski, J. P. M., Kettner, A. J., Overeem, I., Hutton, E. W. H., Hannon, M. T., Brakenridge, G. R., Day, J., Vörösmarty, C., Saito, Y., Giosan, L., & Nicholls, R. J. (2009). Sinking deltas due to human activities. *Nature Geoscience, 2*(10), 681–686.
Syvitski, J. P. M., & Saito, Y. (2007). Morphodynamics of deltas under the influence of humans. *Global and Planetary Change, 57*(3–4), 261–282.
Tan, G., Fang, H., Dey, S., & Wu, W. (2018). Rui-jin zhang's Research on sediment transport. *Journal of Hydraulic Engineering, 144*(6), 02518002.
Thomas, C. G., Spearman, J. R., & Turnbull, M. J. (2002). Historical morphological change in the mersey estuary. *Continental Shelf Research, 22*(11), 1775–1794.
Vellinga, N. E., Hoitink, A. J. F., van der Vegt, M., Zhang, W., & Hoekstra, P. (2014). Human impacts on tides overwhelm the effect of sea level rise on extreme water levels in the Rhine–Meuse delta. *Coastal Engineering, 90*, 40–50.
Walling, D. E., & Fang, D. (2003). Recent trends in the suspended sediment loads of the world's rivers. *Global and Planetary Change, 39*(1–2), 111–126.
Wang, Z. B., Jeuken, M. C. J. L., Gerritsen, H., Vriend, H. J. D., & Kornman, B. A. (2002). Morphology and asymmetry of the vertical tide in the Westerschelde estuary. *Continental Shelf Research, 22*(17), 2599–2609.
Wei, W., Dai, Z., Mei, X., Liu, J. P., Gao, S., & Li, S. (2017). Shoal morphodynamics of the Changjiang (Yangtze) Estuary: Influences from river damming, estuarine hydraulic engineering and reclamation projects. *Marine Geology, 386*, 32–43.
Winterwerp, J. C. (2001). Stratification effects by cohesive and noncohesive sediment. *Journal of Geophysical Research: Oceans, 106*(C10), 22559–22574.
Winterwerp, J. C., Wang, Z. B., van Braeckel, A., van Holland, G., & Kösters, F. (2013). Man-induced regime shifts in small estuaries—II: A comparison of rivers. *Ocean Dynamics, 63*(11–12), 1293–1306.
Wu, T., & Wu, H. (2018). Tidal mixing sustains a bottom-trapped river plume and buoyant coastal current on an energetic continental shelf. *Journal of Geophysical Research: Oceans, 123*(11), 8026–8051.
Wu, H., Zhu, J., Chen, B., & Chen, Y. (2006). Quantitative relationship of runoff and tide to saltwater spilling over from the north Branch in the changjiang estuary: A numerical study. *Estuarine, Coastal and Shelf Science, 69*(1–2), 125–132.
Xie, W., He, Q., Zhang, K., Guo, L., Wang, X., Shen, J., & Cui, Z. (2017). Application of terrestrial laser scanner on tidal flat morphology at a typhoon event timescale. *Geomorphology, 292*, 47–58.
Xie, X., Wang, Z. Y., & Melching, C. S. (2009). Formation and evolution of the Jiuduansha Shoal over the past 50 years. *Journal of Hydraulic Engineering, 135*(9), 741–754.
Yang, H. F., Yang, S. L., Meng, Y., Xu, K. H., Luo, X. X., Wu, C. S., & Shi, B. W. (2018). Recent coarsening of sediments on the southern Yangtze subaqueous delta front: A response to river damming. *Continental Shelf Research, 155*, 45–51.
Yun, C. (1983). Souring and siltation process of tidal flats of the Changjiang estuary and sediment exchange between flats and channels. *Journal of Sedimentary Research, 4*, 45–54. *(In Chinese)*
Yun, C. (2004). *Recent evolution of the Yangtze estuary and its mechanisms*. Beijing, China: China Ocean Press. *(In Chinese)*
Zhao, J., Guo, L., He, Q., Wang, Z. B., van Maren, D. S., & Wang, X. (2018). An analysis on half century morphological changes in the Changjiang Estuary: Spatial variability under natural processes and human intervention. *Journal of Marine Systems, 181*, 25–36.
Zhu, C., Guo, L., Maren, D. S., Tian, B., Wang, X., He, Q., & Wang, Z. B. (2019). Decadal morphological evolution of the mouth zone of the Yangtze Estuary in response to human interventions. *Earth Surface Processes and Landforms, 44*(12), 2319–2332.
Zhu, L., He, Q., Shen, J., & Wang, Y. (2016). The influence of human activities on morphodynamics and alteration of sediment source and sink in the Changjiang Estuary. *Geomorphology, 273*, 52–62.